Preprints of the 21st IFAC World Congress (Virtual)
Berlin, Germany, July 12-17, 2020

Trajectory planning with obstacle avoidance for a concrete pump using harmonic potentials

Julian Wanner * **Felix Brändle** * **Oliver Sawodny** *

* *Institute for System Dynamics, University of Stuttgart, Germany (e-mail: wanner@isys.uni-stuttgart.de, st141597@stud.uni-stuttgart.de, sawodny@isys.uni-stuttgart.de).*

Abstract: The operation of concrete pumps is increasingly supported by assistance systems. They facilitate the complex control task and reduce the risk of accidents. In this paper a trajectory planner for point-to-point motion of a concrete pump is presented. The method is based on harmonic artificial potentials to plan the tool center point motion in the task space and constrained quadratic optimization to convert the task space motion into the configuration space. The algorithm is validated by simulation for a five-link concrete pump.

Keywords: large-scale manipulator, path and trajectory planning, obstacle avoidance, robot manipulators, human operator support, mobile concrete pump

1. INTRODUCTION

Concrete pumps are used worldwide for economical placing of concrete at construction sites. The concrete is pumped through a pipe along the large-scale manipulator. At the tip the hose man guides the concrete onto the site. The operator remotely controls the multiple axis manipulator and navigates the tip of the boom across the construction site. This process is increasingly supported by assistance systems which not only facilitate the complex control task but also reduce the risk of accidents at the construction site, see Benckert (1991), Nissing et al. (1999), Henikl et al. (2015).

Various methods and algorithms can be found for the motion planning of manipulators. Sampling-based planers such as probabilistic roadmaps, Kavraki et al. (1996) and randomly exploring trees, LaValle and Kuffner (2001) probe the configuration space with sampling methods to find a collision free path. Combinatorial based methods such as retraction, O'Dunlaing et al. (1983) and cell decomposition, Schwartz and Sharir (1983) represent the free configuration space with maps and cells. These representations are then used for path planning. Optimal trajectory planning, Gerdts et al. (2012), Schulman et al. (2014) casts the system dynamics and constraints as an optimization problem. The solution gives a collision free trajectory, which also minimizes an optimization criteria.

In general, these methods are not suited for the present problem because their computational requirements and computing times increase significantly with high degrees of freedom of the system and multiple obstacles in 3D task space.

Artificial potential (AP) approaches can efficiently deal with high dimensional manipulators by planning in the task space and transforming the result into the configuration space, Khatib (1986). The method is based on attractive and repulsive potentials, which pull and push the manipulator to the goal position, avoid collisions and enforce constraints. The main drawback of AP is the existence of local minima. They stall the algorithm in the planning process. Harmonic potential functions alleviate this problem by introducing extrema free potentials. For a point mobile robot this approach even guarantees a minimum free solution of the motion problem, Kim and Khosla (1992). In case of nonpoint manipulators the condition does not hold anymore, but the number of local minima is significantly reduced. This is especially true for the typical work setting of a concrete pump at the construction site.

Harmonic potential functions originate from the solutions of differential equations in fluid mechanics. In Kim and Khosla (1992) the panel method is used to efficiently construct harmonic potentials for obstacles in the task space. The resulting AP algorithm utilizes inverse differential kinematics to transform the solution into the configuration space. The method is tested by simulation for a planar multiple link manipulator. Other AP motion planners with harmonic functions for manipulators can be found in Connolly and Grupen (1993), Lau et al. (2012), Fahimi et al. (2003). In the references the harmonic AP method is validated for low dimensional or structural different manipulators in planar environments.

In this paper a trajectory planner for point-to-point motion of the tool-center-point (TCP) of a concrete pump is presented. The system supports the operator with elementary and repetitive sub tasks, avoids obstacles at the construction site and takes system specific constraints into account. For real-time implementation, the algorithm needs to be efficient enough to run on the electronic control unit of the truck. We show an application of the harmonic AP for a high dimensional manipulator in a 3D environment. The algorithm in Kim and Khosla (1992) is extended by introducing a new kinematic transformation method.

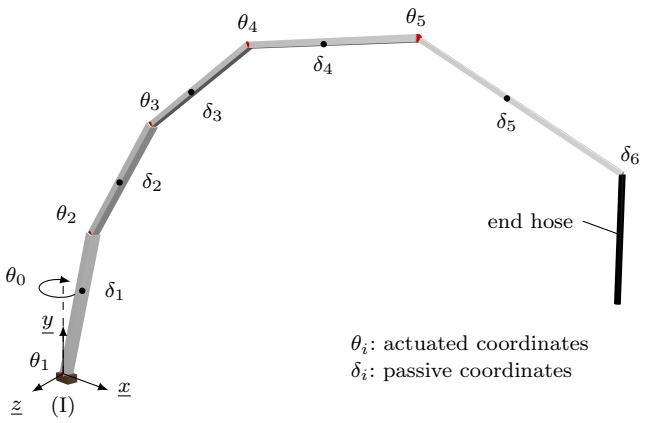

Fig. 1. Manipulator of the concrete pump.

Instead of using an analytic expression for the inverse kinematics, a constraint quadratic optimization problem (cQP) is solved. With this approach various system and environment constraints can be efficiently included into the motion planning algorithm. In addition to that, the cQP separates desired specifications and constraints. The desired specifications are realized through minimization, while strictly complying with the constraints. The formulation allows deviations from the desired values to avoid singularities and meet the constraints.

In the proposed algorithm, obstacles are assumed to be stationary and their position and shape are known. This information is obtained from models of the construction site, such as the building information model, Azhar (2011).

The trajectories are generated at every time step in real-time, forming the motion rate control algorithm from Whitney (1969). The resulting trajectories then serve as the setpoint for the lower level feedback controllers at the joints.

The paper is structured as follows: In Section 2 the kinematic model of the concrete pump is presented. Section 3 describes the AP method and the construction of the harmonic functions. The cQP with different constraints is summarized in Section 4. The method is validated by simulation in Section 5.

2. KINEMATIC MANIPULATOR MODEL

Fig. 1 shows the manipulator of the concrete pump. The five boom links are connected by single degree of freedom revolute joints $\theta_i,\ i = 1,\dots 5$ about the horizontal $\underline{z}$-axis. The revolute joint θ_0 at the base rotates the boom around the $\underline{y}$-axis. A double acting hydraulic cylinder drives the horizontal revolute joints using a mechanical linkage (cylinder and linkage are not shown in Fig. 1). The horizontal joint at the base is actuated by a hydraulic rotary motor with a gearbox. The coordinates $\boldsymbol{\theta} \in \mathbb{R}^6$ are labeled as the actuated coordinates. The elasticity of each link in the vertical plane is represented by virtual revolute joints δ_i. The end hose at the tip of the boom is always parallel to the $\underline{y}$-axis

$$\delta_6 = -\sum_{i=1}^{5}\theta_i - \sum_{i=1}^{5}\delta_i - \frac{\pi}{2}. \tag{1}$$

The coordinates of the virtual joints and the end hose are named the passive coordinates $\boldsymbol{\delta} \in \mathbb{R}^6$, because their value is dependent on the actuated coordinates. The generalized coordinates $\boldsymbol{q} = \begin{bmatrix}\boldsymbol{\theta}^T & \boldsymbol{\delta}^T\end{bmatrix}^T \in \mathbb{R}^{12}$ enclose all given coordinates.

Further information about the virtual joints and the complete model of the concrete pump can be found in Wanner and Sawodny (2019a).

The differential forward kinematics of the tool-center point (TCP) are given as

$$\boldsymbol{v}_{\text{tcp}} = \boldsymbol{J}^{\text{tcp}}(\boldsymbol{q})\dot{\boldsymbol{q}}, \tag{2}$$

where $\boldsymbol{v}_{\text{tcp}} \in \mathbb{R}^3$ is the translational velocity of the end hose tip defined with respect to the inertial frame (I) and $\boldsymbol{J}^{\text{tcp}}$ is the TCP Jacobian matrix.

The Jacobian in (2) can be divided into an actuated and a passive part

$$\boldsymbol{v}_{\text{tcp}} = \boldsymbol{J}_{\theta}^{\text{tcp}}(\boldsymbol{q})\dot{\boldsymbol{\theta}} + \boldsymbol{J}_{\delta}^{\text{tcp}}(\boldsymbol{q})\dot{\boldsymbol{\delta}}, \tag{3}$$

where the Jacobians $\boldsymbol{J}_{\theta}^{\text{tcp}}(\boldsymbol{q})$ and $\boldsymbol{J}_{\delta}^{\text{tcp}}(\boldsymbol{q})$ describe the influence of the actuated and passive velocities $\dot{\boldsymbol{\theta}},\ \dot{\boldsymbol{\delta}}$ on the TCP velocity $\boldsymbol{v}_{\text{tcp}}$.

The same relationship as in (2) and (3) can be found for other points on the manipulator such as the joints or arbitrary points on the segments.

3. ARTIFICIAL POTENTIAL METHOD AND HARMONIC FUNCTIONS

The AP method uses the gradients of a total potential field to guide a point from the starting position to the goal position. The total potential field thereby represents a superposition of different harmonic potential functions. Sink potentials attract, while source potentials repel. In the following an overview of the harmonic potentials for the goal position (sink) as well as the obstacles (sources) is presented. Details can be found in Kim and Khosla (1992) and (Fahimi et al., 2009, p. 111).

The goal potential with respect to the position $\boldsymbol{x}$ is defined as

$$\phi(\boldsymbol{x}) = -\frac{\lambda_{\text{g}}}{\|\boldsymbol{x} - \boldsymbol{x}_g\|}, \tag{4}$$

where $\boldsymbol{x}_{\text{g}}$ is the goal position and $\lambda_{\text{g}} > 0$ defines the strength of the potential. The gradient (A.1) of this function approaches infinity as $\boldsymbol{x}$ gets close to the goal position $\boldsymbol{x}_g$. Conversely, it fades for increasing distances to $\boldsymbol{x}_g$.

Due to the decreasing influence outside the target region, the goal potential is strengthened by a uniform flow

$$\phi(\boldsymbol{x}) = -U\boldsymbol{v}^T\boldsymbol{x}, \tag{5}$$

where $\boldsymbol{v} = \frac{\boldsymbol{x}_{\text{g}} - \boldsymbol{x}_0}{\|\boldsymbol{x}_{\text{g}} - \boldsymbol{x}_0\|}$ is the unit vector from start $\boldsymbol{x}_0$ to end $\boldsymbol{x}_{\text{g}}$ and $U > 0$ is the strength of the potential. The uniform flow potential decreases linearly along the direction of the flow $\boldsymbol{v}$.

The potential field for the obstacles is based on the panel method. This method originates form fluid dynamics and calculates the potential flow of a fluid around bodies of arbitrary shape, Kim and Khosla (1992). The obstacle

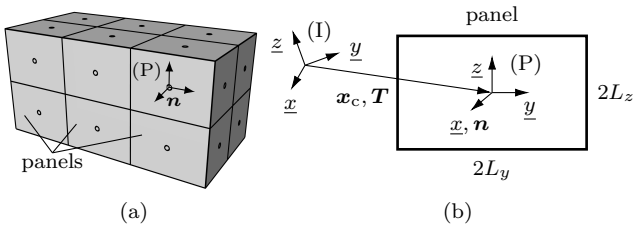

Fig. 2. Rectangular panels approximate obstacles (a) approximated cuboid obstacle (b) single panel.

is thereby approximated by small flat areas or panels as seen in Fig. 2a. Each panel has a distributed source singularity with a uniform density, which deflects the oncoming stream. The trajectory of a fluid particle in the stream serves as the desired motion for the TCP of the manipulator.

In the following, the panel shape will be restricted to rectangular areas. This leads to simpler and more efficient expressions and is sufficient for most obstacles at the construction site. A derivation for panels with arbitrary shape can be found in Fahimi (2008).

A rectangular panel with unit-strength is given by

$$\bar{\bar{\phi}}(\boldsymbol{x}) = -a \int_{-L_y}^{L_y} \int_{-L_z}^{L_z} \frac{1}{\sqrt{x_x^2 + b^2 + c^2}} \,\mathrm{d}l_z \,\mathrm{d}l_y, \qquad (6)$$

$$a = \frac{1}{4\pi}, \quad b = x_y - l_y, \quad c = x_z - l_z,$$

where $\boldsymbol{x} = [x_x \;\; x_y \;\; x_z]^T$ and $2L_y$ and $2L_z$ are the width and height of the rectangle and l_y, l_z the integration variables in the $\underline{y}$ and $\underline{z}$ direction of the local panel coordinate system (P) in Fig. 2b. The center of the panel is at the local origin and the normal $\boldsymbol{n}$ points in the direction of the $\underline{x}$-axis.

Translation and rotation of the panel (6) leads to

$$\bar{\phi}(\boldsymbol{x}) = \bar{\bar{\phi}}(\boldsymbol{T}(\boldsymbol{x} - \boldsymbol{x}_\mathrm{c})), \qquad (7)$$

where $\boldsymbol{x}_\mathrm{c}$ is the center point and $\boldsymbol{T}$ an orthogonal transformation matrix with $\det(\boldsymbol{T}) = 1$ from the intertial system (I) to the rotated local panel coordinate system (P) (see Fig. 2b).

Superposition of the goal potential (4), the uniform flow (5) and m panels (7) yields the total potential field

$$\phi(\boldsymbol{x}) = \phi_\mathrm{g} + \phi_\mathrm{u} + \sum_{i=1}^{m} \lambda_i \bar{\phi}_i, \qquad (8)$$

where λ_i is the strength of the i-th panel.

In order to successfully deflect a fluid particle at a panel, the strength λ_i must be selected such that the normal velocity of the panel cancels or reverses the velocity of the arriving particle. The remaining tangential velocity of the panel then carries the particle around the panel. Depending on the value of the normal velocity, a safety distance around obstacle can be established. This requirement leads to the conditions

$$\left.\frac{\partial \phi}{\partial \boldsymbol{n}_i}\right|_{\boldsymbol{x}=\boldsymbol{x}_{\mathrm{c},i}} = -V_i, \quad i = 1, \ldots, m, \qquad (9)$$

where the $V_i > 0$ is the normal velocity of the i-th panel in the direction $\boldsymbol{n}_i$. The variable V_i determines the repulsion at the panel and thus the safety distance. Note that conditions (9) only determines the necessary strength of the panels at the center $\boldsymbol{x}_{\mathrm{c},i}$.

The m conditions (9) can be transformed into a linear system of equations, cf. (Fahimi, 2008, p. 120)

$$\boldsymbol{P}\boldsymbol{\Lambda} = -\boldsymbol{V} + \boldsymbol{W}, \qquad (10)$$

where

$$P_{ij} = \begin{cases} \frac{1}{2}\pi, & \text{if } i = j, \\ \boldsymbol{n}_i^T \nabla \bar{\phi}_j(\boldsymbol{x}_{\mathrm{c},i}) & \text{if } i \neq j, \end{cases} \qquad (11)$$

$$W_i = -\boldsymbol{n}_i^T \nabla \phi_\mathrm{u}(\boldsymbol{x}_{\mathrm{c},i}) - \boldsymbol{n}_i^T \nabla \phi_\mathrm{g}(\boldsymbol{x}_{\mathrm{c},i}), \qquad (12)$$

$$\boldsymbol{\Lambda} = [\lambda_1 \;\; \lambda_2 \;\; \ldots \;\; \lambda_m]^T, \qquad (13)$$

$$\boldsymbol{V} = [V_1 \;\; V_2 \;\; \ldots \;\; V_m]^T. \qquad (14)$$

The cases for the coordinates of $\boldsymbol{P}$ in (11) are necessary because the gradient in the center of the panel is not defined. Instead the limiting value $\frac{1}{2}\pi$ on the outside of the panel is taken, Kim and Khosla (1992).

To ensure a continous flow towards the goal with a single global minimum for the total potential function, the condition

$$-\lambda_\mathrm{g} < \lambda_\mathrm{o} < 0, \qquad (15)$$

$$\lambda_\mathrm{o} = \sum_{i=1}^{m} \lambda_i A_i = \boldsymbol{\Lambda}^T \boldsymbol{A}, \qquad (16)$$

$$\boldsymbol{A} = [A_1 \;\; A_2 \;\; \ldots \;\; A_m]^T \qquad (17)$$

must be satisfied, cf. Kim and Khosla (1992), where λ_o is the combined obstancle strength and A_i the area of the panel i.

The selection of suitable V_i depends on the position, number and area of the panels as well as on the points $\boldsymbol{x}_0$ and $\boldsymbol{x}_\mathrm{g}$. Every time one of the latter parameter changes, a new V_i needs to be found. The method in Fahimi et al. (2009) simplifies this process by automatically selecting the V_i such that condition (15) is met. The vector $\boldsymbol{V}$ is thereby chosen proportional to the area of the panels

$$\boldsymbol{V} = k\boldsymbol{A}, \qquad (18)$$

where $k > 0$ is a scalar. Applying (18) to (10) and solving for $\boldsymbol{\Lambda}$ leads with (16) to λ_o. Using (15) an upper bound for k can be found

$$k < k_\mathrm{max} = \frac{\lambda_g + \boldsymbol{A}^T \boldsymbol{P}^{-1} \boldsymbol{W}}{\boldsymbol{A}^T \boldsymbol{P}^{-1} \boldsymbol{A}}. \qquad (19)$$

Normalizing k leads to the safety region

$$r_\mathrm{k} = \frac{k}{k_\mathrm{max}}, \quad 0 < r_\mathrm{k} < 1. \qquad (20)$$

With the parameters λ_g, U, r_k, $\boldsymbol{x}_0$ and $\boldsymbol{x}_\mathrm{g}$, the necessary strength of the panels $\boldsymbol{\Lambda}$ is calculated. The negative gradient of the total potential (A.7) then gives the desired local velocity $\hat{\boldsymbol{v}}_\mathrm{tcp}$ of the manipulator TCP in the task space. For stationary obstacles the inverse $\boldsymbol{P}^{-1}$ stays constant for different goal positions $\boldsymbol{x}_\mathrm{g}$. This property increases the computational efficiency especially for a high number of obstacles.

4. CONSTRAINT QUADRATIC OPTIMIZATION

The cQP transforms the desired TCP velocities $\hat{\boldsymbol{v}}_\mathrm{tcp}$ into the joint velocities in the configuration space by solving the

inverse differential kinematics with additional constraints. The formulation is based on Knierim and Sawodny (2015) and Wanner and Sawodny (2019b).

The optimization problem is defined as

$$\min_{\dot{\boldsymbol{\theta}}} \|\hat{\boldsymbol{v}}_{\mathrm{tcp}} - \boldsymbol{J}_{\mathrm{g}}^{\mathrm{tcp}}(\boldsymbol{q})\dot{\boldsymbol{\theta}}\|_{\boldsymbol{W}_{\hat{v}}} + \|\dot{\hat{\boldsymbol{\theta}}} - \dot{\boldsymbol{\theta}}\|_{\boldsymbol{W}_{\hat{\theta}}} + \|\dot{\boldsymbol{\theta}}\|_{\boldsymbol{W}_{\theta}} \quad (21a)$$

subject to

$$\underline{\dot{\boldsymbol{\theta}}} \leq \quad \dot{\boldsymbol{\theta}} \quad \leq \overline{\dot{\boldsymbol{\theta}}}, \quad (21b)$$

$$\boldsymbol{C}(\boldsymbol{q})\dot{\boldsymbol{\theta}} \leq \overline{\boldsymbol{v}}, \quad (21c)$$

where $\dot{\boldsymbol{\theta}}$ is the optimization variable, $\hat{\boldsymbol{v}}_{\mathrm{tcp}}$ is the desired TCP velocity, $\boldsymbol{W}_{\hat{v}} \in \mathbb{R}^{3\times3}$, $\boldsymbol{W}_{\hat{\theta}}, \boldsymbol{W}_{\theta} \in \mathbb{R}^{6\times6}$ are the positive definite weighing matrices, $\boldsymbol{J}_{\mathrm{g}}^{\mathrm{tcp}} \in \mathbb{R}^{3\times6}$ is the manipulator Jacobian (with deformation compensation), $\dot{\hat{\boldsymbol{\theta}}}$ is the desired joint velocity, $\underline{\dot{\boldsymbol{\theta}}}$, $\overline{\dot{\boldsymbol{\theta}}}$ are the lower and upper velocity bounds and $\boldsymbol{C}$ is the matrix of the general inequality constraints with the upper bound $\overline{\boldsymbol{v}}$.

The equation (21a) contains three different objectives. The first term minimizes the difference between the desired and the actual TCP velocity. It thus realizes the inverse kinematic calculation. The closeness to $\hat{\boldsymbol{v}}_{\mathrm{tcp}}$ can be controlled via the weighing matrix $\boldsymbol{W}_{\hat{v}}$. The second term utilizes the redundant degrees of freedom of the manipulator to implement an additional movement in the nullspace of the configuration space. The third term acts as a damping factor to reduce actuation energy and to improve the numerical conditioning of the problem.

The cQP is solved at every time step with the desired TCP velocities form the AP algorithm. It selects the optimal joint velocities to follow $\hat{\boldsymbol{v}}_{\mathrm{tcp}}$ and complies with all given constraints. The active set solver qpOASES Ferreau et al. (2014) is used to solve the cQP, which is designed for embedded and online applications.

In the following subsections, an overview of the various constraints and requirements of the concrete pump and their cQP formulation is given. Details can be found in the stated references.

Configuration control Due to the redundant nature, the manipulator can reach a point in the task space with different configurations. To prevent drift and maintain the configuration after collision avoidance, the cQP has a configuration control. The method uses the second term in the objective function (21a) to set a desired configuration $\hat{\boldsymbol{\theta}}$ with

$$\dot{\hat{\boldsymbol{\theta}}} = \boldsymbol{K}(\hat{\boldsymbol{\theta}} - \boldsymbol{\theta}), \quad (22)$$

where $\boldsymbol{K}$ is a diagonal matrix with gain factors. The resulting velocity $\dot{\hat{\boldsymbol{\theta}}}$ is weighted weakly to avoid interference with the main objective.

Deformation compensation The manipulator of the concrete pump is vulnerable to elastic deformation in the links. This effect depends on gravity, the structure and the mass distribution of the links and the posture. The rigid body motion of the manipulator is therefore superimposed by the static nonlinear deformation, which leads to faulty distance calculations in the collision detection.

In Wanner and Sawodny (2019b) a deformation compensation algorithm is proposed, which is used in the following. The method utilizes a dynamic model of the manipulator to calculate the static deformation of the passive joints depending on the actuated coordinates

$$\boldsymbol{\delta} = \boldsymbol{f}_{\delta}(\boldsymbol{\theta}). \quad (23)$$

By differentiating (23) with respect to time yields with (3) the deformation compensated Jacobian

$$\boldsymbol{v}_{\mathrm{tcp}} = (\boldsymbol{J}_{\theta}^{\mathrm{tcp}} + \boldsymbol{J}_{\delta}^{\mathrm{tcp}} \frac{\partial \boldsymbol{f}_{\delta}}{\partial \boldsymbol{\theta}})\dot{\boldsymbol{\theta}} := \boldsymbol{J}_{\mathrm{g}}^{\mathrm{tcp}}\dot{\boldsymbol{\theta}}. \quad (24)$$

The passive joint δ_6 of the end hose is treated analogously, where the relationship (23) is given by (1).

The deformation compensated Jacobian (24) can be found for other arbitrary points on the manipulator.

Hydraulic flow rate constraints The hydraulic system of the concrete pump is designed to run only three actuators at full speed at the same time. This approach allows small-sized and energy efficient components in the system. As a result, there is not enough hydraulic fluid for each actuator in dynamic phases of the trajectory planning. The manipulator therefore deviates unexpectedly from the desired trajectory.

To prevent this behavior an upper bound on the total hydraulic flow rate is implemented in the cQP. The constraint has the weighted L_1-norm structure

$$k_{\mathrm{h}0}|\dot{\theta}_0| + k_{\mathrm{h}1}|\dot{\theta}_1| + \cdots + k_{\mathrm{h}5}|\dot{\theta}_5| \leq \overline{Q}_{\mathrm{h}}, \quad (25)$$

where $k_{\mathrm{h}i}$ are constants depending on the parameters of the hydraulic system and $\overline{Q}_{\mathrm{h}}$ is the upper bound of the flow rate. Details of the flow rate constraint can be found in Wanner and Sawodny (2019b).

Joint constraints The box constraints (21b) realize joint specific requirements with the upper and lower limits $\underline{\dot{\boldsymbol{\theta}}}$, $\overline{\dot{\boldsymbol{\theta}}}$. For the current problem position and velocity constraints according to Knierim and Sawodny (2015) are implemented.

Obstacle constraints The desired motion $\hat{\boldsymbol{v}}_{\mathrm{tcp}}$ from the AP algorithm gives a collision free trajectory for the TCP without considering the manipulator links. The cQP must therefore contain a link-obstacle collision avoidance. For this purpose the velocity of the nearest link point to the obstacle is reduced such that the link comes to a stop at the boundary. By bounding the velocity only in the direction of the shortest distance, the constraint exerts minimal impact on the remaining movement. The obstacle constraint j is

$$\boldsymbol{e}_j^T \boldsymbol{J}_{\mathrm{g}}^{j}(\boldsymbol{q})\dot{\boldsymbol{\theta}} \leq \overline{v}_j, \quad (26)$$

where $\boldsymbol{e}_j$ is the unit vector of the shortest distance (see Fig. 3)

$$\boldsymbol{e}_j = \frac{\boldsymbol{x}_{\mathrm{o},j} - \boldsymbol{x}_{\mathrm{m},j}}{\|\boldsymbol{x}_{\mathrm{o},j} - \boldsymbol{x}_{\mathrm{m},j}\|}, \quad (27)$$

$\boldsymbol{J}_{\mathrm{g}}^{j}$ is the deformation compensated Jacobian of the nearest point $\boldsymbol{x}_{\mathrm{m},j}$ on the link and $\overline{v}_j$ is the breaking velocity, cf. Knierim and Sawodny (2015)

$$\overline{v}_j = \begin{cases} \sqrt{-2\underline{a}(d_j - d_{\min})} & \text{if } d_j \geq d_{\min}, \\ 0 & \text{if } d_j < d_{\min}, \end{cases} \quad (28)$$

with the specified braking acceleration $\underline{a} < 0$, the current distance d_j and the safety distance $d_{\min}$ to the obstacle. In this paper the links of the manipulator are approximated by connected line segments. The obstacles are modeled as

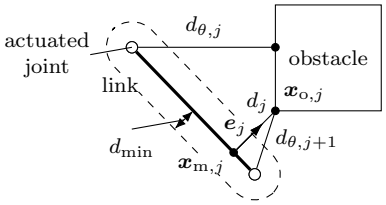

Fig. 3. Shortest distance between link and obstacle (2D scheme).

oriented 3D bounding boxes. The proximity calculations are based on the analytic approaches from Schneider (2003). Note that the safety distance $d_{\min}$ effectively leads to a bounding capsule for the manipulator links.

The collision avoidance calculates the distance between each segment and every obstacle and selects the shortest distances per link. These distances are then constrained in the cQP. To avoid abrupt changes in the constraints when a new obstacle comes close, the shortest distance of every actuated joint to the obstacles $d_{\theta,j}$ is also constrained with the same approach (see Fig. 3).

Self-collision constraint Self-collision avoidance of the manipulator is similar to the obstacle constraints. In contrast to stationary obstacles, the manipulator links move with respect to each other. To avoid collision, the relative motion between the links in the direction of the shortest distance is restricted. The corresponding constraint has the structure (26), where the Jacobian is replaced by the relative Jacobian of the nearest point pair on the links j and i

$$\boldsymbol{J}^{\mathrm{rel},j} = \boldsymbol{J}^{j} - \boldsymbol{J}^{i}. \tag{29}$$

The proximity query thereby consists of the shortest distance calculation between two line segments according to Schneider (2003).

5. SIMULATION RESULTS

The trajectory planning algorithm with the harmonic AP and the cQP is simulated for the concrete pump of Section 2. The task space settings represent a potential scenario at the construction site. The manipulator must traverse a cuboid obstacle while avoiding a low hanging ceiling. Fig. 4 and Fig. 5 depict the scenario in the task space. The start configuration $\boldsymbol{\theta}_0 = [60\ 90\ 0\ -50\ -90\ -30]^T$ deg and the TCP end goal $\boldsymbol{x}_{\mathrm{g}} = [20\ 3\ 15]^T$ m are selected such that a simultaneous movement of the rotary motor and cylinders are necessary. Panels with size 7.5 m × 7.5 m represent obstacle and ceiling in the AP. The safety parameter r_{k} is 0.3, which allows a movement close to the obstacle, but is robust enough to deal with the finite number of boundary conditions (9). The cQP contains all the features described in Section 4. The configuration control has the parameters $\hat{\boldsymbol{\theta}} = \boldsymbol{\theta}_0$ and $\boldsymbol{K} = \boldsymbol{I}$ with the unit matrix $\boldsymbol{I}$. The obstacle constraints have the safety distance $d_{\min} = 1$ m and the braking acceleration $\underline{a} = -5 \times 10^{-2}\,\mathrm{m/s^2}$. The algorithm works at a sampling rate of $T_{\mathrm{s}} = 20$ ms.

As illustrated in Fig. 4 and Fig. 5, the proposed algorithm successfully solves the given task. The resulting TCP path shows a smooth progression with a predictable motion. The predictability helps the operator to monitor the movement. The trajectories at joint level are shown

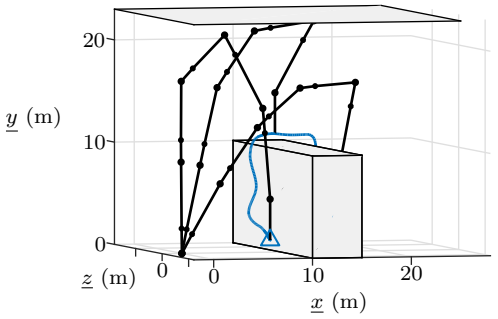

Fig. 4. TCP path (—) and manipulator with actuated and virtual joints (•—•) at start (▵), middle and goal (□) position in task space with cuboid obstacle and ceiling.

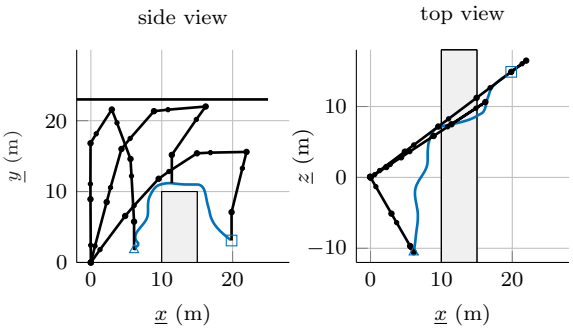

Fig. 5. Side and top view of Fig. 4.

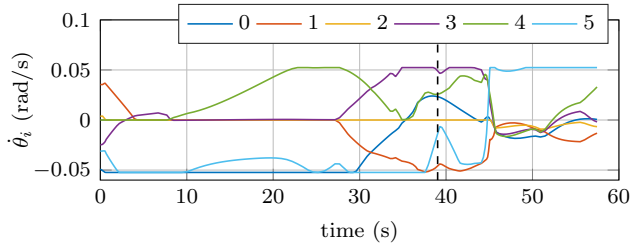

Fig. 6. Actuated joint velocities $\dot{\theta}_i,\ i = 0, \ldots, 5$ of TCP movement shown in Fig. 4.

in Fig. 6. The velocity bounds are clearly noticeable. The dashed line at $t = 39$ s represent the manipulator in the middle position as drawn in Fig. 4. Although the ceiling constrains the vertical velocity, the horizontal movement of the manipulator is not influenced. That is why the horizontal movement of the fourth link in the narrow space between ceiling and obstacle is possible (see Fig. 5, side view).

As noted before, the proposed method is not free of local minima. But the number of minima are greatly reduced. A distinctive local minima, which occurs easily is the alignment of the end hose and the joint axis θ_0. This is shown in Fig. 7, where the dashed line represents the latter axis. Since the manipulator is driven by the desired TCP velocities this local minimal stops the movement around the θ_0 axis (see red TCP path). The problem is easily fixed by introducing a virtual obstacle in the AP, which diverts the TCP from the critical axis (see blue TCP path).

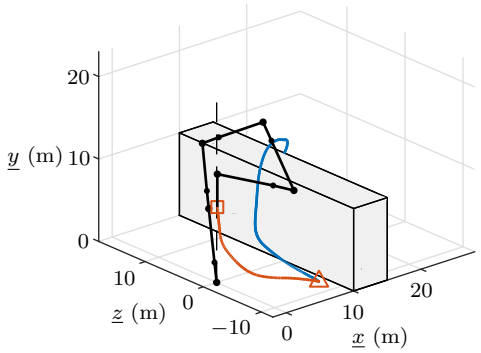

Fig. 7. TCP path with (—) and without (—) singularity avoidance in the task space and manipulator with actuated an virtual joints (•—•) in singular configuration.

6. CONCLUSION

In this paper a trajectory planning algorithm for a concrete pump is presented. The method is based on harmonic AP and a cQP to transform the desired TCP velocities into the configuration space. The framework incorporates various constraints and requirements of the concrete pump in configuration and task space, such as obstacle avoidance, deformation compensation and hydraulic flow rate constraints. The efficient structure of the method enables online implementation on the electronic control unit of the truck. The simulation shows the successful implementation for a potential task at the construction site.

ACKNOWLEDGEMENTS

This work was supported by the Liebherr-Mischtechnik GmbH.

REFERENCES

Azhar, S. (2011). Building information modeling (bim): Trends, benefits, risks, and challenges for the aec industry. *Leadership and management in engineering*, 11(3), 241–252.

Benckert, H. (1991). Computer controlled concrete distribution. In *Proc. 8th Int. Symp. on Automation and Robotics in Construction*, 111–118.

Connolly, C.I. and Grupen, R.A. (1993). The applications of harmonic functions to robotics. *Journal of Robotic Systems*, 10(7), 931–946.

Fahimi, F. (2008). *Autonomous robots: modeling, path planning, and control*, volume 107. Springer Science & Business Media.

Fahimi, F., Ashrafiuon, H., and Nataraj, C. (2003). Obstacle avoidance for spatial hyper-redundant manipulators using harmonic potential functions and the mode shape technique. *Journal of Field Robotics*, 20(1), 23–33.

Fahimi, F., Nataraj, C., and Ashrafiuon, H. (2009). Real-time obstacle avoidance for multiple mobile robots. *Robotica*, 27(2), 189–198.

Ferreau, H.J., Kirches, C., Potschka, A., Bock, H.G., and Diehl, M. (2014). qpoases: A parametric active-set algorithm for quadratic programming. *Mathematical Programming Computation*, 6(4), 327–363.

Gerdts, M., Henrion, R., Hömberg, D., and Landry, C. (2012). Path planning and collision avoidance for robots. *Numerical Algebra, Control and Optimization*, 2(3), 437–463.

Henikl, J., Kemmetmüller, W., and Kugi, A. (2015). Estimation and control of the tool center point of a mobile concrete pump. *Automation in Construction*.

Kavraki, L.E., Svestka, P., Latombe, J.C., and Overmars, M.H. (1996). Probabilistic roadmaps for path planning in high-dimensional configuration spaces. *IEEE transactions on Robotics and Automation*, 12(4), 566–580.

Khatib, O. (1986). Real-time obstacle avoidance for manipulators and mobile robots. *The international journal of robotics research*, 5(1), 90–98.

Kim, J.O. and Khosla, P.K. (1992). Real-time obstacle avoidance using harmonic potential functions. *IEEE Transactions on Robotics and Automation*, 8(3), 338–349.

Knierim, K.L. and Sawodny, O. (2015). Tool-Center-Point control of the KAI manipulator using constrained QP optimization. *Mechatronics*, 30, 85–93.

Lau, D., Eden, J., and Oetomo, D. (2012). Motion planning of a planar 3r manipulator utilising fluid flow trajectory generation. In *Proc. Australasian Conference on Robotics and Automation, New Zealand*.

LaValle, S.M. and Kuffner, J.J. (2001). Rapidly-exploring random trees: Progress and prospects. *Algorithmic and Computational Robotics: New Directions*, 293–308.

Nissing, D., Bernzen, W., and Schwarz, H. (1999). On vibration control of a concrete pump. In *1999 European Control Conference (ECC)*, 4514–4519.

O'Dunlaing, C., Sharir, M., Yap, C.K., et al. (1983). Retraction: A new approach to motion-planning. In *Proceedings of the fifteenth annual ACM symposium on Theory of computing*, 207–220. ACM.

Schneider, P. (2003). *Geometric tools for computer graphics*. Boston Morgan Kaufmann Publishers, Amsterdam.

Schulman, J., Duan, Y., Ho, J., Lee, A., Awwal, I., Bradlow, H., Pan, J., Patil, S., Goldberg, K., and Abbeel, P. (2014). Motion planning with sequential convex optimization and convex collision checking. *The International Journal of Robotics Research*, 33(9), 1251–1270.

Schwartz, J.T. and Sharir, M. (1983). On the piano movers problem. ii. general techniques for computing topological properties of real algebraic manifolds. *Advances in applied Mathematics*, 4(3), 298–351.

Wanner, J. and Sawodny, O. (2019a). A lumped parameter model of the boom of a mobile concrete pump. In *2019 European Control Conference (ECC)*.

Wanner, J. and Sawodny, O. (2019b). Tool-center-point control of a flexible link concrete pump with hydraulic limitations using quadratic programming. In *IEEE International Conference on Automation Science and Engineering (CASE)*.

Whitney, D.E. (1969). Resolved motion rate control of manipulators and human prostheses. *IEEE Transactions on man-machine systems*, 10(2), 47–53.

Appendix A. PARTIAL DERIVATIVES OF GOAL, UNIFORM AND PANEL POTENTIAL

$$\nabla\phi_\mathrm{g} = \lambda_g \frac{\boldsymbol{x}-\boldsymbol{x}_g}{\|\boldsymbol{x}-\boldsymbol{x}_\mathrm{g}\|^3}, \tag{A.1}$$

$$\nabla\phi_\mathrm{u} = -U\boldsymbol{v}, \tag{A.2}$$

$$\nabla\bar{\phi} = \boldsymbol{T}^T\nabla\bar{\bar{\phi}}(\boldsymbol{T}(\boldsymbol{x}-\boldsymbol{x}_\mathrm{c})), \tag{A.3}$$

$$\frac{\partial\bar{\bar{\phi}}}{\partial x_x} = a\arctan\left(\frac{bc}{x_x d}\right)\Big|_{l_z=-L_z}^{l_z=L_z}\Big|_{l_y=-L_y}^{l_y=L_y}, \tag{A.4}$$

$$\frac{\partial\bar{\bar{\phi}}}{\partial x_y} = a\ln\left(-c-d\right)|_{l_z=-L_z}^{l_z=L_z}\Big|_{l_y=-L_y}^{l_y=L_y}, \tag{A.5}$$

$$\frac{\partial\bar{\bar{\phi}}}{\partial x_z} = a\ln\left(-b-d\right)|_{l_z=-L_z}^{l_z=L_z}\Big|_{l_y=-L_y}^{l_y=L_y}, \tag{A.6}$$

$$a=\frac{1}{4\pi},\quad b=(x_y-l_y),\quad c=(x_z-l_z),$$
$$d=\sqrt{x_x^2+b^2+c^2},$$

$$\nabla\phi = \nabla\phi_\mathrm{g}+\nabla\phi_\mathrm{u}+\sum_{i=1}^{m}\lambda_i\nabla\bar{\phi}_i. \tag{A.7}$$